Chemosphere 307 (2022) 136068

Contents lists available at ScienceDirect

Chemosphere

journal homepage: www.elsevier.com/locate/chemosphere

Polyaspartic acid enhances the Cd phytoextraction efficiency of *Bidens pilosa* by remolding the rhizospheric environment and reprogramming plant metabolism

Xiong Li [a,b,c,1], Liyan Tian [d,1], Boqun Li [e], Huafang Chen [a,b], Gaojuan Zhao [a,b], Xiangshi Qin [c], Yuanyuan Liu [c], Yongping Yang [c,f,**], Jianchu Xu [a,b,*]

[a] *Center for Mountain Futures, Kunming Institute of Botany, Chinese Academy of Sciences, Kunming, 650201, China*
[b] *Department of Economic Plants and Biotechnology, Yunnan Key Laboratory for Wild Plant Resources, Kunming Institute of Botany, Chinese Academy of Sciences, Kunming, 650201, China*
[c] *Germplasm Bank of Wild Species, Kunming Institute of Botany, Chinese Academy of Sciences, Kunming, 650201, China*
[d] *School of Energy and Environment Science, Yunnan Normal University, Kunming, 650500, China*
[e] *Science and Technology Information Center, Kunming Institute of Botany, Chinese Academy of Sciences, Kunming, 650201, China*
[f] *Xishuangbanna Tropical Botanical Garden, Chinese Academy of Sciences, Xishuangbanna, 666303, China*

HIGHLIGHTS

- PASP added in soils significantly enhanced plant growth and Cd uptake in *B. pilosa*.
- PASP recruited many PGPR in the rhizosphere of *B. pilosa*.
- PASP and KSR highly activated available K in the rhizosphere of *B. pilosa*.
- Organic acids, amino acids, and lipids contributed to Cd detoxification in *B. pilosa*.

GRAPHICAL ABSTRACT

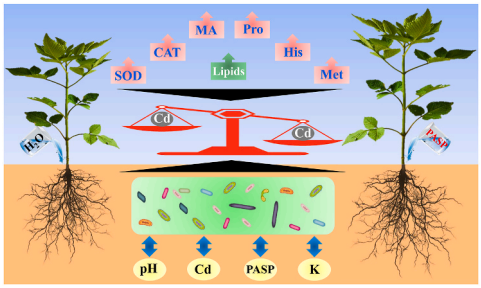

ARTICLE INFO

Handling Editor: T Cutright

ABSTRACT

The green soil chelator polyaspartic acid (PASP) can enhance heavy metal phytoextraction efficiency, but the potential mechanisms are not clearly understood from the whole soil–plant system. In this study, we explored the effects and potential mechanisms of PASP addition in soils on plant growth and cadmium (Cd) uptake in the Cd

Abbreviations: ACd, available Cd; ACu, available Cu; AFe, available Fe; AK, available K; AP, available P; AZn, available Zn; BCF, bioconcentration factor; CA, citric acid; CAT, catalase; Cd, cadmium; Cu, copper; EC, electrical conductivity; EDTA, ethylenediaminetetraacetic acid; EMg, exchangeable Mg; Fe, iron; HN, hydrolysable N; HRP, horseradish peroxidase; ICP–OES, inductively coupled plasma–optical emission spectrometry; K, potassium; KSR, K solubilizing rhizobacteria; LDA, linear discriminate analysis; MA, malic acid; MDA, malondialdehyde; Mg, magnesium; N, nitrogen; OTU, operational taxonomic unit; P, phosphorus; PASP, polyaspartic acid; Pb, lead; PGPR, plant growth-promoting rhizobacteria; PCA, principal component analysis; RDA, redundancy analysis; ROS, reactive oxygen species; SOD, superoxide dismutase; TF, translocation factor; UPLC–ESI–MS/MS, ultra-performance liquid chromatography–electrospray ionization tandem mass spectrometry; Zn, zinc.

** Corresponding author. 132# Lanhei Road, Kunming, 650201, China.
* Corresponding author. 132# Lanhei Road, Kunming, 650201, China.
E-mail addresses: yangyp@mail.kib.ac.cn (Y. Yang), jxu@mail.kib.ac.cn (J. Xu).
[1] These authors contributed equally to this work.

https://doi.org/10.1016/j.chemosphere.2022.136068
Received 4 April 2022; Received in revised form 17 July 2022; Accepted 10 August 2022
Available online 16 August 2022

Keywords:
Heavy metal
Phytoremediation
Soil chelator
Plant metabolomics
Rhizobacteria

hyperaccumulator *Bidens pilosa* by analysing variations in chemical elements, rhizospheric microbial community, and plant metabolomics. The results showed that PASP significantly promoted the biomass yield and Cd concentration in *B. pilosa*, leading to an increase in the total accumulated Cd by 46.4% and 76.4% in shoots and 124.7% and 197.3% in roots under 3 and 6 mg kg^{-1} PASP addition, respectively. The improved soil-available nutrients and enriched plant growth-promoting rhizobacteria (e.g., *Sphingopyxis, Sphingomonas, Cupriavidus, Achromobacter, Nocardioides,* and *Rhizobium*) were probably responsible for the enhanced plant growth after PASP addition. The increase in Cd uptake by plants could be due to the improved rhizosphere-available Cd, which was directly activated by PASP and affected by the induced rhizobacteria involved in immobilizing/mobilizing Cd (e.g., *Sphingomonas*, *Cupriavidus*, *Achromobacter*, and *Rhizobium*). Notably, PASP and/or these potassium (K)-solubilizing rhizobacteria (i.e., *Sphingomonas, Cupriavidus,* and *Rhizobium*) highly activated rhizosphere-available K to enhance plant growth and Cd uptake in *B. pilosa*. Plant physiological and metabolomic results indicated that multiple processes involving antioxidant enzymes, amino acids, organic acids, and lipids contributed to Cd detoxification in *B. pilosa.* This study provides novel insights into understanding how soil chelators drive heavy metal transfer in soil–plant systems.

1. Introduction

Phytoextraction, an effective phytoremediation technique, is widely used for the removal of heavy metals from contaminated soils by harvesting the aerial parts of heavy metal accumulators or hyperaccumulators (Wang et al., 2022). Although multiple excellent plant species (e.g., heavy metal hyperaccumulators) have been identified and used for phytoextraction (Reeves et al., 2018), the phytoextraction efficiency can be restricted by the low bioavailability of heavy metals in soils and/or small plant biomass limited by soil nutrients. Thus, a crucial strategy for enhancing phytoextraction efficiency is to improve the bioavailability of heavy metals and/or soil nutrients in soils, which can be achieved by two main routes: (1) application of soil chelators and (2) regulation of plant rhizosphere microecosystems (Yu et al., 2020; Wang et al., 2021a).

Chelators, which mainly include low molecular weight organic acids and aminopolycarboxylic acids, are effective soil amendments that can enhance phytoextraction efficiency (Dolev et al., 2020; Thinh et al., 2021). At present, the potential mechanisms by which soil chelators promote heavy metal accumulation in plants mainly involve three aspects: (1) activating the bioavailability of immobilized heavy metals; (2) stimulating the structure and activity of plant roots for the improved absorption of heavy metal ions or chelates; and (3) increasing the tolerance and bearing capacity of plants to heavy metals or their chelates (He et al., 2019). As some traditional chelators, such as ethylenediaminetetraacetic acid (EDTA), are difficult to degrade in soils, which can lead to secondary pollution to the environment, green chelators used for enhancing phytoextraction efficiency have attracted substantial attention in recent years (He et al., 2019; Arshad et al., 2020).

Polyaspartic acid (PASP) is a completely biodegradable polymer that is widely used in environmental and agricultural fields. Previous studies have shown that PASP can enhance the nutrient uptake, growth rate, and biomass yield of plants (Deng et al., 2019; Ji et al., 2021). PASP has also been demonstrated to act as a soil chelator to enhance the phytoextraction efficiency of heavy metals in several recent studies (He et al., 2019; Liu et al., 2019; Li et al., 2020a; Wang et al., 2021b). He et al. (2019) found that PASP significantly improved plant growth and Cd accumulation, resulting in an increase in accumulated Cd and Pb in *Solanum nigrum* shoots and roots. Liu et al. (2019) reported that nickel (Ni) absorption in *Bidens pilosa* was significantly promoted by the chelating agents PASP and aminotriacetic acid. Li et al. (2020a) found that PASP treatment could not only significantly increase the biomass of *Pennisetum* sp. but also maintained a high Cd uptake capacity by activating the stable fractions. Wang et al. (2021b) reported that the addition of PASP increased Cd accumulation in stems and roots of *Iris sibirica* and exhibited better comprehensive efficacy than humic acid, rhamnolipid, and sodium tripolyphosphate. These studies jointly confirmed the promoting effect of PASP on heavy metal phytoextraction efficiency, but none of them explored the potential mechanisms. As PASP has many carboxyl and hydroxyl groups that can chelate heavy metals (Hou et al., 2020), the direct activation of heavy metal bioavailability by PASP in soils should be a main reason for PASP enhancing heavy metal accumulation in plants (Wang et al., 2020a). However, adding PASP to soil means that PASP likely interacts with other soil factors, leading to multiple processes and effects. For example, Liu et al. (2019) found that the addition of PASP significantly improved the activities of microorganisms in soils. Many rhizospheric microorganisms can mitigate the negative effects of Cd on plants or influence the chemical forms and bioavailability of Cd (Khanna et al., 2019; Manoj et al., 2020; Yuan et al., 2021), which directly determine Cd accumulation levels in plants. Therefore, we wondered whether and how PASP interacts with other soil factors, especially with the soil microbial community, to affect heavy metal phytoextraction. Moreover, the mechanism by which plants coordinate their growth and increase heavy metal uptake under PASP addition is unclear. In this study, we explored the effects of PASP on plant growth and Cd accumulation in the potential Cd hyperaccumulator *B. pilosa* (Zhang et al., 2021) in a Cd-contaminated soil. On this basis, we analysed changes in the physiological and metabolic responses of *B. pilosa* and the dynamics of the rhizosphere soil microecosystem under PASP addition. The results of this study can help us understand the mechanisms by which PASP enhances Cd phytoextraction efficiency in the entire soil–plant system and provide theoretical guidance to further improve the phytoextraction efficiency in Cd-polluted soils.

2. Materials and methods

2.1. Preparation of experimental materials

Mature seeds of *B. pilosa* were collected from the Kunming Botanical Garden (Kunming, China). The PASP solid reagent was purchased from Shanghai Macklin Biochemical Co., Ltd. (Macklin, Shanghai, China).

Cd-polluted soils from an earlier study (Li et al., 2021b) were used for the experiments. After being sieved through a 4-mm sieve, the soils were mixed to obtain a homogeneous soil mixture. The basic parameters of this homogenized soil (pH: 5.51; organic matter: 213 g kg^{-1}; electrical conductivity (EC): 588 μS cm^{-1}; total nitrogen (N): 7.55 g kg^{-1}; total phosphorus (P): 1.13 g kg^{-1}; total Cd: 19.0 mg kg^{-1}; total copper (Cu): 18.0 mg kg^{-1}; total zinc (Zn): 96.0 mg kg^{-1}) were analysed.

2.2. Experimental design

Seeds of uniform plumpness and size were first surface sterilized and cleaned using a previously described method (Li et al., 2021c). The sterilized seeds were then germinated in Cd-free soils in a temperature- and humidity-controlled greenhouse (Li et al., 2021b). The homogenized soil samples were divided into 2.0 kg (wet weight) aliquots placed into flowerpots ($h = 17.5$ cm, $d = 18.5$ cm) with a uniform height of 17 cm. The flowerpots were placed on impermeable plastic trays to hold the

leachate. After 2 weeks of sowing, *B. pilosa* seedlings of the same size were transferred into flowerpots (four seedlings per pot) and placed in the same greenhouse for 20 days. Based on the dry weight of the soil in the pots, the plants were divided into three groups that were separately treated with 0 (0P), 3 (3P), and 6 g kg^{-1} (6P) PASP. The PASP dosages were chosen based on previously reported studies (Zhang et al., 2013, 2019c). PASP was added to the soil samples twice at an interval of 1 week, in accordance with previous methods (He et al., 2019; Zhang et al., 2019c). For each addition, half the amount of PASP for the targeted dosages was dissolved in 150 ml of deionized water and poured evenly around the plant roots. Deionized water was used for the control (0P) group. This liquid amount prevented leakage from the bottom of the flowerpot. The experiment ended after one month of plant growth following the first PASP addition. Three biological replicates for each treatment were analysed for all parameters.

2.3. Sample collection and biomass measurement

The second and third leaves from the top of *B. pilosa* plants for each treatment were collected and stored at −80 °C to detect their physiological indices. To measure biomass and element concentrations, the roots and shoots of *B. pilosa* plants were harvested separately. Root samples were cleaned following a previously described method (Wu et al., 2018). The plant samples were oven-dried at 80 °C for 48 h and then weighed. Moreover, the rhizospheric soil, which naturally adheres to the root systems after hand shaking corresponding to each plant sample (Li et al., 2022b), was collected and stored at −80 °C to measure the physicochemical indices and microbial community composition.

2.4. Detection of Cd and nutrient element concentrations in plants

The concentrations of Cd, Cu, Zn, and iron (Fe) in *B. pilosa* shoots and/or roots were measured using inductively coupled plasma–mass spectrometry as described previously (Li et al., 2017). The digestion processes of all these elements were identical, but they were identified and quantified according to their respective detection wavelengths and standard curves.

The Cd bioconcentration factor (BCF), translocation factor (TF), and total Cd accumulation in the shoots and roots of *B. pilosa* plants in a pot were calculated as previously described (Li and Yang, 2020).

The concentrations of magnesium (Mg) in plant shoots were detected by inductively coupled plasma–optical emission spectrometry (ICP–OES). In brief, approximately 0.5 g samples were digested by 5 mL HNO_3 under a temperature gradient (100 °C, 3 min; 140 °C, 3 min; 160 °C, 3 min; 180 °C, 3 min; 190 °C, 15 min). The digestion solutions were then transferred to a 50 ml volumetric flask, and the volume was fixed using ultrapure water. The Mg concentrations were detected using an inductively coupled plasma spectrometer (Optima 8000, PerkinElmer, US).

The concentrations of total N in plant shoots were detected by the micro-Kjeldahl method. In brief, approximately 0.5 g samples were added to 0.4 g $CuSO_4$, 6 g K_2SO_4, and 20 ml H_2SO_4 in the digestion tube for digestion. When the temperature reached 420 °C (the liquid in the digestion tube appeared blue–green and clear), the mixture continued to digest for 1 h. The digestion tube was removed, cooled, added to 20 ml water, and then distilled for 7 min on an automatic Kjeldahl nitrogen analyser (Haineng K9840, Jinan, China). The distillate was injected into a receiving bottle with 1–2 drops of indicator mixture (volume ratio of 1 g L^{-1} methyl red ethanol solution and 1 g L^{-1} bromocresol green ethanol solution = 1:5) and 10 ml boric acid solution (20 g L^{-1}) to reach 200 mL. The mixture was then titrated to light grayish red with HCl standard solution (0.1 mmol L^{-1}). The total N concentration was calculated according to the corresponding formula.

2.5. Antioxidant system assay

The activities of the antioxidant enzymes superoxide dismutase (SOD) and catalase (CAT), as well as malondialdehyde (MDA) concentrations, in *B. pilosa* leaves were measured using the corresponding assay kits (Solarbio, Beijing, China) as described previously (Li et al., 2021a, 2021c, 2022a).

2.6. Widely targeted metabolomic analysis

Widely targeted metabolomics technology (Chen et al., 2013) was used in this study to understand the metabolic response in *B. pilosa* leaves after PASP addition. The main experimental procedures, including sample preparation and extraction, ultra-performance liquid chromatography–electrospray ionization tandem mass spectrometry (UPLC–ESI-MS/MS) analysis, identification and quantification of metabolites, differential metabolite analysis, and KEGG annotation and enrichment analysis, were performed according to the methods described in previous studies (Chen et al., 2013; Li and Song, 2019; Zhao et al., 2021) that carried out similar metabolomic analysis.

2.7. Determination of soil physicochemical indices

In this study, soil pH and the concentrations of hydrolysable N (HN), available P (AP), K (AK), Cd (ACd), Cu (ACu), Fe (AFe), Zn (AZn), and exchangeable Mg (EMg) were detected using the methods introduced in the corresponding detection standards in China (Guan et al., 2017; Cha et al., 2020; Li et al., 2020b). In short, the soil pH was determined using the potentiometric method (LY/T 1239–1999). Soil HN was hydrolyzed using a 1.8 M NaOH solution, absorbed by a boric acid solution, and then titrated using a 0.01 M HCl standard solution (LY/T 1228–2015). Soil AP (LY/T 1232–2015) and AK (LY/T 1234–2015) were extracted using HCl (0.05 M)-H_2SO_4 (0.025 M) extractant and detected by ICP–OES. Soil EMg was exchanged using an ammonium acetate solution (1 M, pH 7.0) and detected by atomic absorption spectrophotometry (LY/T 1245–1999). The concentrations of available ACd, ACu, AFe, and AZn were extracted from the soils using diethylenetriamine pentaacetic acid-calcium chloride-triethanolamine (DTPA-$CaCl_2$-TEA) buffer solution and then detected by ICP–OES (HJ 804–2016).

2.8. Soil microbial community composition analysis

Soil microbial DNA extraction, 16S rDNA amplification, sequencing, and bioinformatics analyses were performed as previously described (Li et al., 2021b).

2.9. Statistical analyses

Statistical analysis was conducted using the Statistical Package for the Social Sciences (version 18.0). Significant differences (significance level 0.05) among the three groups were determined using one-way analysis of variance (ANOVA) with Tukey's test. Principal component analysis (PCA), correlation analysis, and redundancy analysis (RDA) were performed via the online platform Omicsmart (http://www.omicsmart.com).

3. Results

3.1. Effects of PASP addition on plant growth

As shown in Fig. 1a, the growth status of *B. pilosa* was markedly different in PASP-added (3P and 6P) soils compared to the control (0P) soil. The average biomass yields of *B. pilosa* plants treated with PASP were significantly higher ($p < 0.05$) than those of the control plants for both shoots and roots (Fig. 1b and c). However, the biomass yields of *B. pilosa* plants did not differ significantly between the 3P and 6P groups

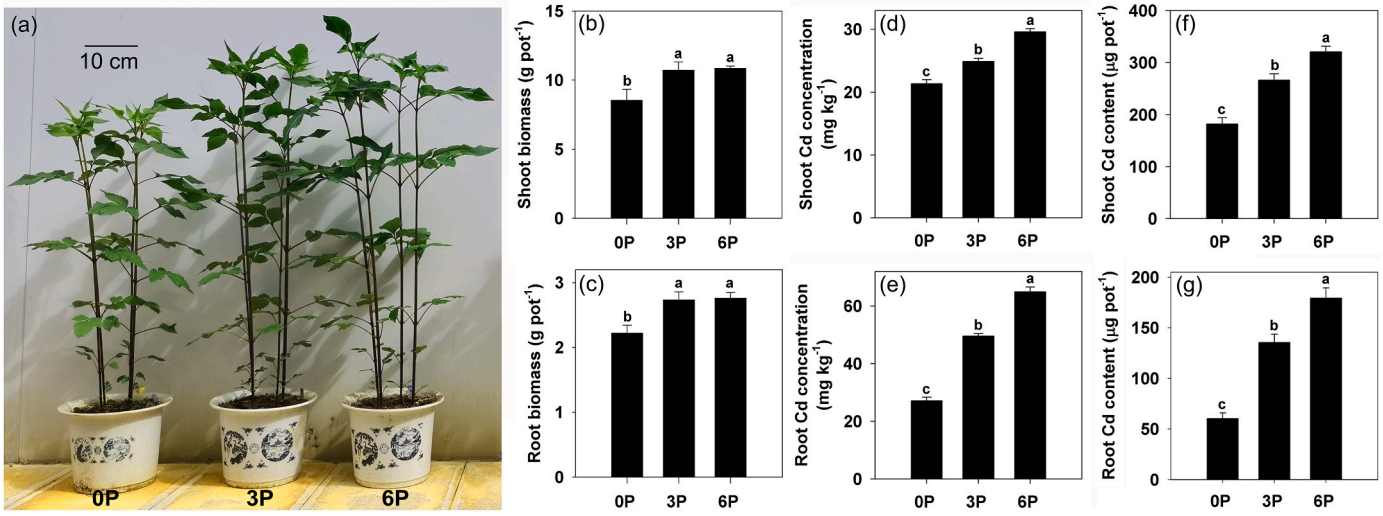

Fig. 1. Plant growth and Cd accumulation characteristics of *Bidens pilosa* growing in Cd-polluted soils supplemented with 0 (0P), 3 (3P), and 6 g kg^{-1} (6P) poly-aspartic acid. **(a)** Representative plant morphology. **(b)** Shoot biomasses (dry weight). **(c)** Root biomasses (dry weight). **(d)** Shoot Cd concentrations (dry weight). **(e)** Root Cd concentrations (dry weight). **(f)** Shoot Cd contents. **(g)** Root Cd contents. Data represent means ± standard deviations (n = 3); bars labelled with different letters indicate significant differences among different groups at the $p < 0.05$ level (**b–g**).

(Fig. 1b and c), indicating that there are potential factors that limit the continuous growth of *B. pilosa* under higher PASP dosages (e.g., 6 g kg^{-1}).

3.2. Effects of PASP addition on Cd accumulation and nutrient intake in *B. pilosa*

In this study, Cd concentrations in both shoots and roots of *B. pilosa* significantly increased ($p < 0.05$) with increasing PASP dosages (Fig. 1d and e), indicating a similar change in the trend of Cd BCFs in both shoots and roots (Supplementary Fig. S1a and b). However, the Cd TFs of the 3P and 6P groups were significantly lower ($p < 0.05$) than those of the 0P group (Supplementary Fig. S1c). As both biomass yields and Cd concentrations increased after PASP addition, the total Cd content accumulated in *B. pilosa* plants significantly increased. In the samples from the 3P and 6P groups, the total Cd contents in the shoots increased by 46.4% and 76.4% ($p < 0.05$), respectively (Fig. 1f), whereas those in roots increased by 124.7% and 197.3% ($p < 0.05$), respectively (Fig. 1g), compared with those in the 0P group.

Compared with the 0P group, the concentrations of several nutrient elements, including macroelements (i.e., N and Mg) and microelements (i.e., Cu, Fe, and Zn), in *B. pilosa* shoots were significantly increased ($p < 0.05$) (Supplementary Table S1).

3.3. Changes in the antioxidant system in leaves of *B. pilosa* under PASP addition

The changes in the antioxidant system were assayed to understand Cd detoxification in *B. pilosa* under PASP addition. Both SOD and CAT activities in the 6P group were significantly higher ($p < 0.05$) than those in the 0P and 3P groups (Supplementary Figs. S2a and b). However, MDA concentrations did not change significantly among the different groups (Supplementary Fig. S2c).

3.4. Metabolomics dynamics in leaves of *B. pilosa*

The UPLC–ESI–MS/MS-based metabolomics approach was used to understand the whole metabolic network of *B. pilosa* under different PASP inoculation dosages. The PCA results showed that the distribution areas of the 0P, 3P, and 6P samples were clearly separated (Fig. 2a), indicating that there were significant changes in the metabolic compositions among the different samples. Overall, 741 metabolites, mainly flavonoids (210), phenolic acids (132), lipids (101), amino acids and derivatives (75), organic acids (58), nucleotides and derivatives (48), etc., were detected and quantified using mass spectrometric data (Fig. 2b; Supplementary Table S2).

Based on the screening conditions for identifying differential metabolites (variable importance-of-the-projection score ≥1 and absolute value of $\log_2$ (fold change) > 1), a total of 120 (84 upregulated and 36 downregulated) and 178 (109 upregulated and 69 downregulated) differential metabolites were identified in the 3P and 6P groups compared to the 0P group, respectively (Supplementary Fig. S3 and Tables S3 and S4). The Venn diagram reflects the common and specific differential metabolites between the 3P and 6P groups. As shown in Fig. 2c, there were 24 and 82 specific differential metabolites in the 3P and 6P groups, respectively. Interestingly, these 96 common differential metabolites (64 upregulated and 32 downregulated) exhibited similar changes in both the 3P and 6P groups (Fig. 2c). These differential metabolites were enriched in a number of KEGG pathways related to substance metabolism and biosynthesis (Supplementary Figs. S4 and S5), indicating that the addition of PASP resulted in the reprogramming of the metabolic process of *B. pilosa*. The number of up- and downregulated metabolites for each substance category in the 3P and 6P groups is shown in Fig. 2d and e. Notably, in both the 3P and 6P groups, the upregulated metabolites belonging to amino acids and derivatives, lipids, and organic acids accounted for more than 80% of the total differential metabolites (Fig. 2d and e), suggesting that they were primarily induced by the addition of PASP.

3.5. Changes in physicochemical indices in rhizospheric soil of *B. pilosa*

To explore the effects of PASP addition on the rhizosphere, we examined the changes in the important indices in the rhizosphere soils of *B. pilosa*. The average rhizosphere pH values (5.81–5.98) were similar among the 0P, 3P, and 6P soils (Supplementary Table S5). In contrast, the EC of the 6P soil was significantly higher ($p < 0.05$) than those of the 0P and 3P soils (Supplementary Table S5). The concentrations of ACd, HN, AP, EMg, ACu, and AFe were not markedly different among the three soils (Supplementary Table S5), whereas the AZn concentrations in the 3P soil were significantly higher ($p < 0.05$) than those in the 0P and 6P soils (Supplementary Table S5). It should be noted that the concentrations of AK in the 3P and 6P soils were 3.7 and 21.7 times higher ($p <$

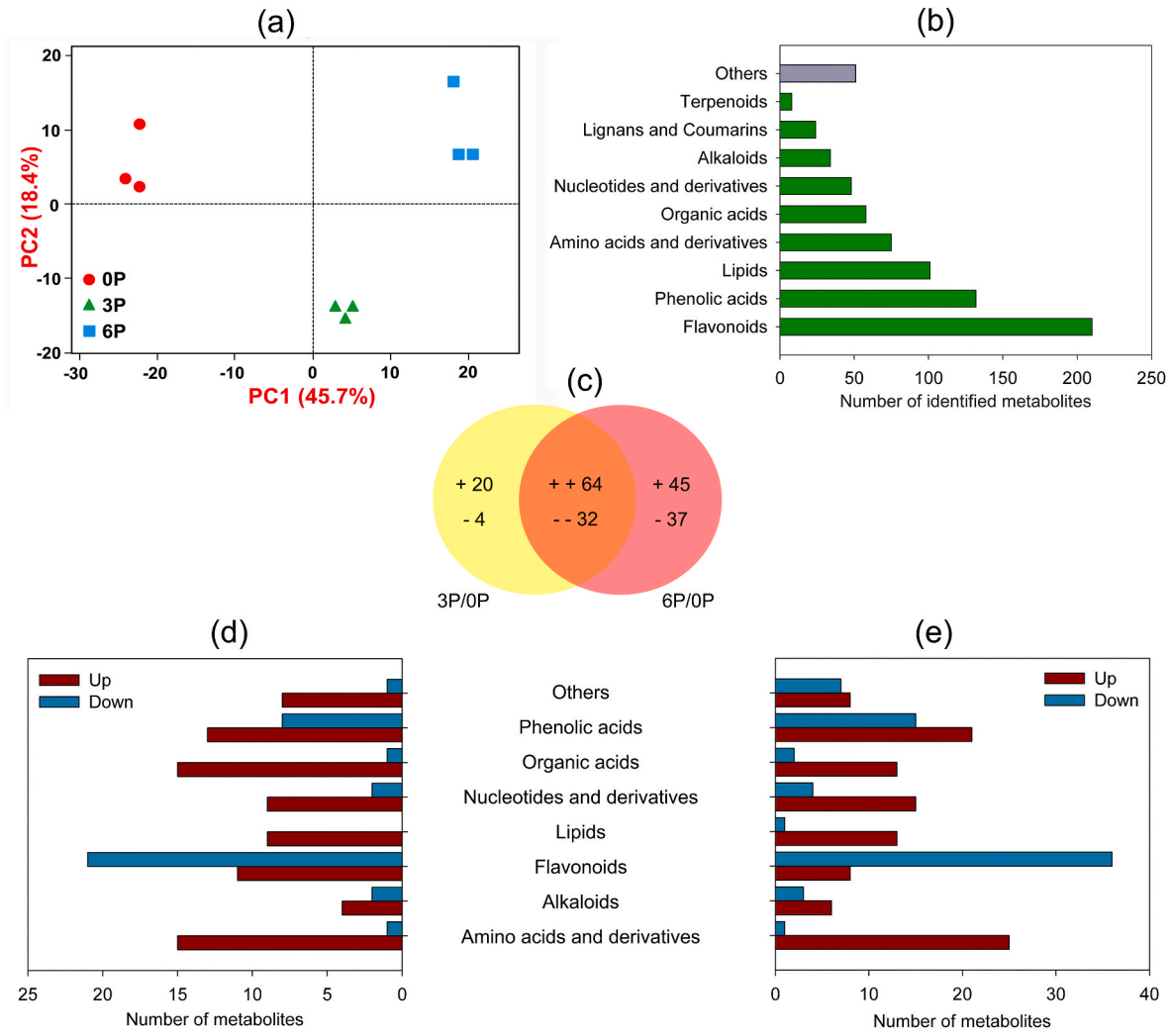

Fig. 2. Widely targeted metabonomic analysis of the leaves of *Bidens pilosa* growing in Cd-polluted soils supplemented with 0 (0P), 3 (3P), or 6 g kg^{-1} (6P) polyaspartic acid. (**a**) Principal component analysis (PCA) of metabonomic data from the three groups. **(b)** Number of identified metabolites for different substance categories. (**c**) Venn diagram of the number of differential metabolites between the 3P and 6P groups compared with the 0P group. '+' and '-' represent increased and decreased metabolites, respectively. (**d**) Number of up- and downregulated metabolites identified in different substance categories in the 3P group. **(e)** Number of up- and downregulated metabolites identified in different substance categories in the 6P group.

0.05), respectively, than that of the 0P soil (Supplementary Table S5).

As shown in Supplementary Fig. S6, the correlation analysis of soil physicochemical properties indicated that these soil properties were divided into two major clusters. Cluster 1 included pH, EMg, ACu, AZn, and AFe, whereas Cluster 2 included EC, AK, PASP, ACd, AP, and HN (Supplementary Fig. S6). Soil indices (excluding HN) in Cluster 2 showed an obvious positive correlation ($p < 0.001$, $0.001 < p < 0.01$, and $p < 0.05$) with each other (Supplementary Fig. S6). These correlations indicate the complex interrelationship among the soil physicochemical properties after PASP addition. Of these, the ACd concentration was significantly positively correlated ($p < 0.05$) with EC and concentrations of AK and PASP but significantly negatively correlated ($p < 0.05$) with pH (Supplementary Fig. S6).

3.6. Variations in microbial community composition in rhizospheric soils of B. pilosa

As soil microorganisms act not only as responders to soil environmental changes but also as promoters of plant growth or heavy metal uptake by plants, 16S rDNA sequencing was employed to analyse the variations in soil bacterial community composition in this study. The raw sequencing reads were deposited into the Sequence Read Archive (SRA) database of NCBI (Accession Number: PRJNA751709), which was released on 2021.12.31.

3.6.1. Analysis of rhizosphere microbial community composition

The number of tags and OTUs obtained from the 16S rDNA sequencing of each sample are shown in Supplementary Table S6. On average, 4868, 4797, and 4812 OTUs were identified in the 0P, 3P, and 6P soils, respectively, which were not significantly different among the three soils (Supplementary Table S6). The three soils shared 2928 core OTUs (Fig. 3a), which accounted for 60.1%–61.0% of their total OTUs. The unique OTUs (580–972) in the three soils (Fig. 3a) accounted for 12.1%–20.0% of their total OTUs. Consistent with similar OTU numbers, none of the alpha indices (i.e., Shannon, Simpson, Chao1, and Ace) showed significant differences among the three soils (Supplementary Table S7).

The number of identified bacterial taxa at different classification levels in the soil is shown in Supplementary Fig. S7, and the relative abundance of the top 19 bacterial phyla with a relative abundance > 0.1% in at least one sample is presented in Supplementary Table S8. The abundance of 17 bacterial phyla among the three soils showed a complex correlation network (Fig. 3b). The phyla Patescibacteria (11), Hydrogenedentes (11), Kiritimatiellaeota (11), and Omnitrophicaeota

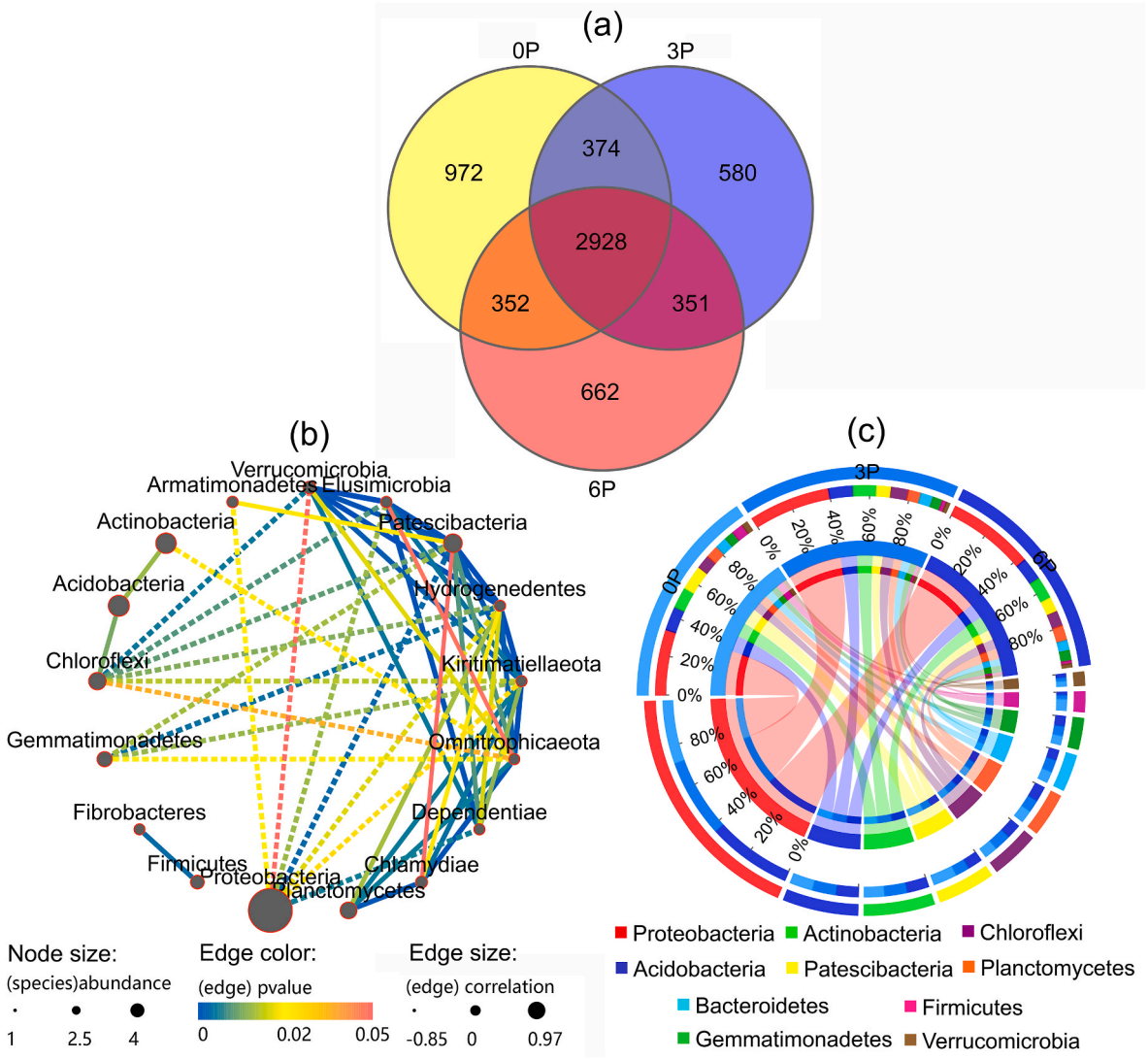

Fig. 3. Microbial community composition based on 16S rDNA sequencing in rhizosphere soils of *Bidens pilosa* supplemented with 0 (0P), 3 (3P), and 6 g kg^{-1} (6P) polyaspartic acid. **(a)** Venn diagram of operational taxonomic units among different soils. **(b)** Pearson correlation network among the top 19 bacterial phyla. The solid and dotted lines represent positive and negative correlations, respectively. **(c)** Circos diagram showing the relative abundance of the top 10 bacterial phyla identified in different soils.

(10) exhibited the highest connectivity (Fig. 3b), indicating that they may affect a large number of other bacterial taxa. The top 10 bacterial phyla followed the order of relative abundance: Proteobacteria (31.0%–41.1%) > Acidobacteria (10.8%–11.6%) > Actinobacteria (10.0%–11.1%) > Patescibacteria (6.9%–11.7%) > Chloroflexi (6.5%–8.1%) > Planctomycetes (6.0%–7.3%) > Bacteroidetes (4.8%–6.0%) > Gemmatimonadetes (4.4%–4.8%) > Firmicutes (1.3%–5.6%) > Verrucomicrobia (1.6%–2.6%), which accounted for approximately 95% of the bacterial abundance in each soil (Fig. 3c; Supplementary Table S8).

3.6.2. *Correlations between soil indices and the soil bacterial community*

RDA was applied to assess the potential correlations between soil indices and bacterial phylum and genus community composition. The top 20 bacterial phyla and bacterial genera were used as response variables. Seven soil indices (i.e., pH, EC, PASP, AZn, ACd, AK, and ACu), which were altered among different soils or potentially affected the soil environment, were used as explanatory variables. As the actual PASP concentrations in the rhizosphere were challenging to measure, the initial addition dosages were used for RDA in this study.

The seven soil indices accounted for 91.03% (first axis: 70.78%, second axis: 20.25%) of the total variation in bacterial phyla (Fig. 4a). The main soil indices affecting the bacterial phylum variation included PASP (envfit analysis, $R^2 = 0.7741$, $p = 0.002$), pH (envfit analysis, $R^2 = 0.8320$, $p = 0.016$), and AK (envfit analysis, $R^2 = 0.5419$, $p = 0.041$) (Fig. 4a; Supplementary Table S9). Approximately 91.3% (first axis: 76.09%, second axis: 15.21%) of the total variation in bacterial genera could be explained by the seven selected variables (Fig. 4b). The main soil indices affecting the bacterial genus variation were PASP (envfit analysis, $R^2 = 0.7299$, $p = 0.025$) and pH (envfit analysis, $R^2 = 0.8310$, $p = 0.026$) (Fig. 4b; Supplementary Table S10). Correlation network analysis largely supported the RDA results. As shown in Fig. 4c, PASP dosage and pH in soils were significantly correlated with the abundance of several bacterial phyla. At the genus level, PASP also had the highest connectivity to the bacteria (Fig. 4d). These results indicate that PASP may directly or indirectly affect other soil indices (e.g., pH and AK) to regulate rhizospheric bacterial composition.

3.6.3. *Variations in rhizobacteria*

Although the alpha indices showed no significant difference among the three soils (Supplementary Table S7), LEfSe analysis showed that the abundance of many specific bacterial taxa was altered (LDA > 2.5) in 3P and 6P soils in comparison with 0P soil (Fig. 5a and b; Supplementary

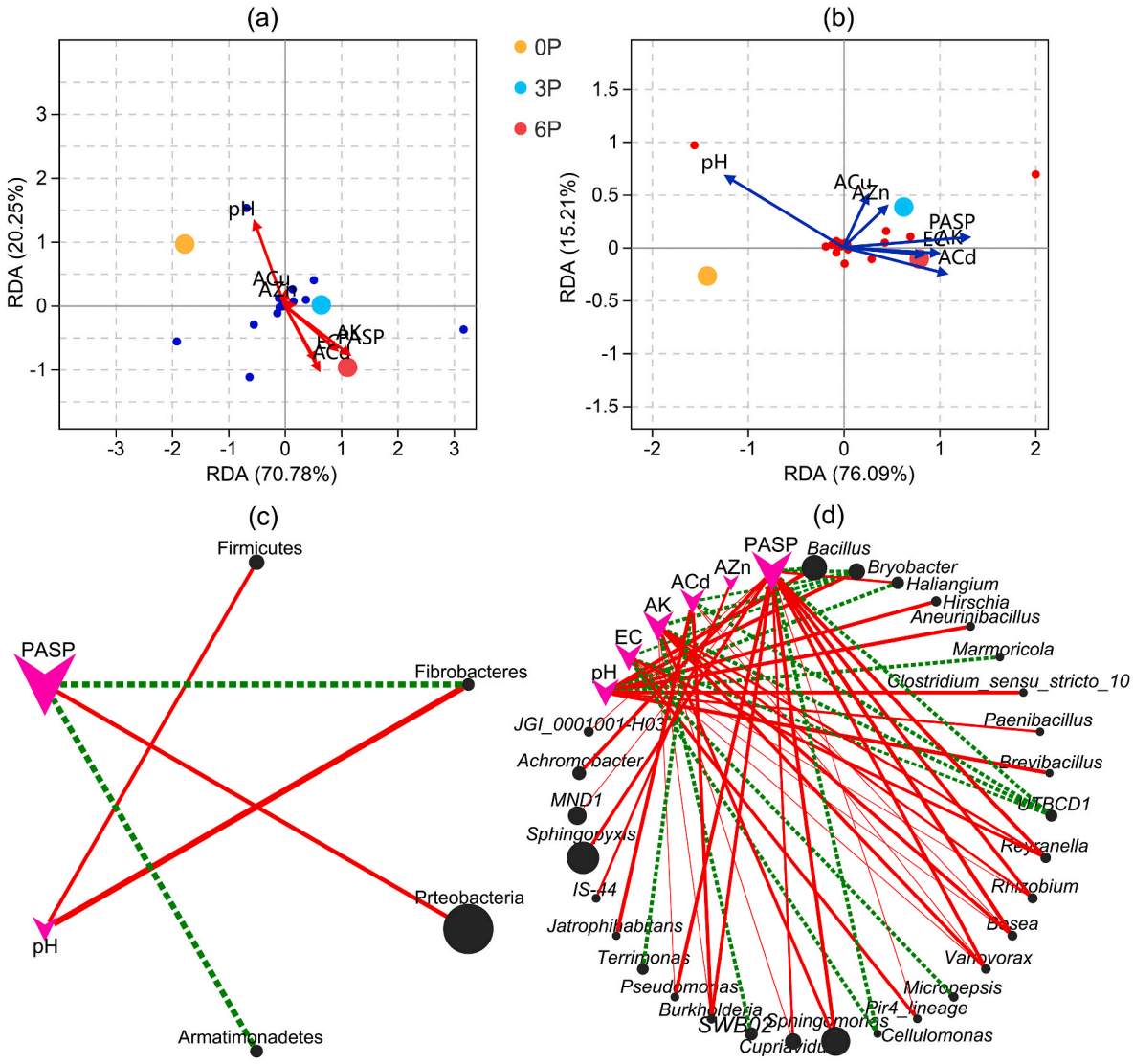

Fig. 4. Redundancy analysis (RDA) and correlation network results showing the correlations between the soil indices and rhizobacteria in rhizospheric soils of *Bidens pilosa* supplemented with 0 (0P), 3 (3P), and 6 g kg^{-1} (6P) polyaspartic acid (PASP). RDA results showing the influence of soil indices on the variation in the bacterial community at the phylum **(a)** and genus (**b**) levels. Correlation network results showing the correlations between soil indices and bacterial phyla **(c)** and genera (**d**). The red solid lines and green dotted lines indicate significantly ($p < 0.05$) positive correlations and negative correlations, respectively; the thickness of lines is negatively correlated with p value; the size of node shapes for environmental factors and bacteria indicate their connectivity and relative abundance, respectively (**c** and **d**). ACd: available Cd; ACu: available Cu; AK: available K; AZn: available Zn; EC: electrical conductivity.

Tables S11 and S12). A total of 33 and 48 bacterial taxa were abundance-altered in the 3P and 6P soils, respectively (Fig. 5c). Among them, 26 bacterial taxa showed consistent change trends in abundance between 3P and 6P soils, whereas 7 and 22 bacterial taxa were separately altered in 3P and 6P soils, respectively (Fig. 5c). Common and specific differential bacteria were observed between 3P and 6P soils at both the phylum and genus levels (Fig. 5d and e). These results indicate the dose effect of PASP on the rhizobacteria of *B. pilosa*.

Further analysis indicated that many of these upregulated bacterial genera in 3P and/or 6P soils belonged to plant growth-promoting rhizobacteria (PGPR) (Fig. 6). Among them, some PGPR were involved in solubilizing/insolubilizing Cd or solubilizing K (Fig. 6). Most of these PGPR were enriched in both 3P and 6P soils, whereas only *Sphingomonas* was specifically enriched in the 6P soil (Fig. 6). These PGPR likely play important roles in promoting Cd phytoextraction efficiency by *B. pilosa*.

4. Discussion

4.1. Application of PASP for enhancing Cd phytoextraction efficiency

The phytoextraction efficiency of heavy metals is determined by both plant biomass and heavy metal concentrations in plants. In this study, PASP addition not only improved the biomass yield of *B. pilosa* but also increased the Cd concentrations in plants, thereby greatly enhancing the Cd phytoextraction efficiency (Fig. 1). These results agree with the promoting effect of PASP on Cd phytoextraction efficiency for several other plant species (Zhang et al., 2013, 2019a, 2019c; He et al., 2019; Xie et al., 2021), suggesting that PASP can act as a universal soil chelator to enhance Cd phytoextraction efficiency.

PASP has minimal adverse effects on soil functions because it is nontoxic and highly susceptible to biodegradation (Mu'azu et al., 2018). Moreover, PASP can be mass produced because of its green chemical synthesis process (e.g., fermentation and thermal polymerization) (Yang et al., 2018). These advantages allow PASP to be practically applied for

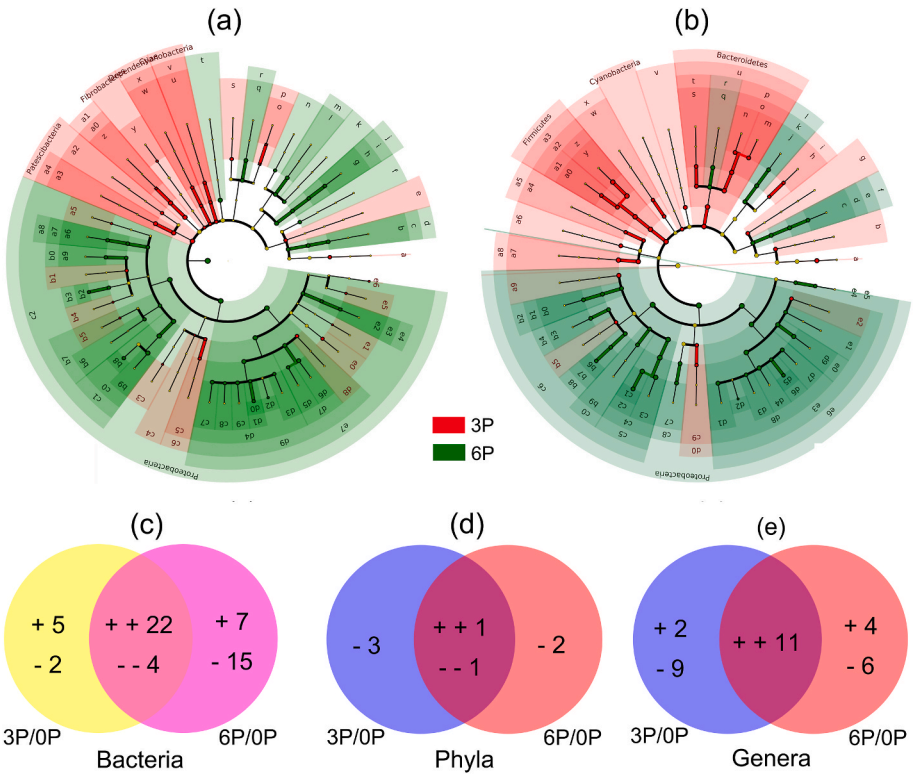

Fig. 5. LEfSe analysis showing indicator bacteria with linear discriminate analysis (LDA) scores >2.5 in rhizospheric soils of *Bidens pilosa* supplemented with 0 (0P), 3 (3P), and 6 g kg^{-1} (6P) polyaspartic acid. **(a)** Cladogram showing the phylogenetic distribution of the indicator bacteria between 0P and 3P soils. The identifiers labelled on the cladogram correspond to those in Supplementary Table S11. **(b)** Cladogram showing the phylogenetic distribution of the indicator bacteria between 0P and 6P soils. The identifiers labelled on the cladogram correspond to those in Supplementary Table S12. The diameter of each circle is proportional to the abundance of the taxa (**a** and **b**). **(c)** Venn diagram of indicator bacteria between 3P and 6P soils compared with the 0P soil. **(d)** Venn diagram of indicator bacterial phyla between 3P and 6P soils compared with the 0P soil. **(e)** Venn diagram of indicator bacterial genera between 3P and 6P soils compared with the 0P soil. "+" and "-" represent up- and downregulated bacterial taxa in 3P and 6P soils, respectively (**c**–**e**).

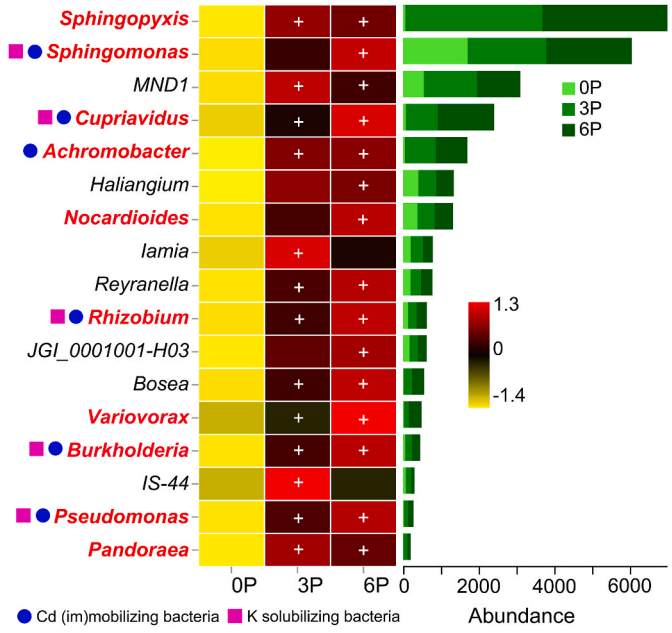

Fig. 6. Dynamic heatmap and stacked map showing bacterial genera enriched in rhizospheric soils of *Bidens pilosa* supplemented with 3 (3P) and 6 g kg^{-1} (6P) polyaspartic acid in comparison with the control soil (0P). The relative abundance of bacteria used is normalized at the row level for heatmap. Plus (+) signs indicate the bacteria enriched in 3P and/or 6P soils. Bacterial genera in red bold font indicate plant growth-promoting rhizobacteria, and bacterial genera labelled with blue circles and pink squares indicate bacteria involved in mobilizing/immobilizing Cd and solubilizing K, respectively.

enhancing Cd phytoextraction efficiency. However, the results of this study showed that greater amounts of PASP did not continue to increase plant biomass yields (Fig. 1a–c). This may be attributed to the fact that more Cd accumulated in the plants and began to inhibit plant growth under higher PASP addition. Alternatively, an overdose in PASP addition may cause high N stress for plants to inhibit plant growth according to a previous study (Cao et al., 2021). Therefore, the application of PASP should be controlled within a reasonable dose range to maximize the Cd phytoextraction efficiency. The optimal PASP dosage for specific soil–plant systems needs to be investigated practically.

In this study, PASP addition was found to significantly remodel the rhizospheric environment (Fig. 5) and reprogram the plant metabolism of *B. pilosa* (Fig. 2). These results indicate that there are complex processes that regulate plant growth, Cd uptake, and Cd detoxification in *B. pilosa* under PASP addition.

4.2. Mechanisms of growth improvement in B. pilosa under PASP addition

Nutrient elements are the basis of plant growth and development. In this study, the uptake of both macroelements (i.e., N and Mg) and microelements (i.e., Cu, Fe, and Zn) in *B. pilosa* shoots was enhanced under PASP addition (Supplementary Table S1), which conformed to the increased biomass yields of *B. pilosa* plants. These results can be interpreted as PASP effectively enhances the availability of soil nutrients through its adsorption and chelation function (Cao et al., 2021; Ji et al., 2021). In addition to the potential activation effect of PASP on N nutrition, the degradation of PASP in soils may directly provide an N source for plants. However, in the rhizospheric soils, the available/exchangeable fractions of most nutrient elements (i.e., N, P, Mg, Cu, and Fe) did not change with increasing PASP dosages (Supplementary Table S5). This can be attributed to trade-offs among the activation, immobilization, and intake by organisms (including plants and microbes) for these elements under different dosages of PASP addition. It should be noted that soil K availability was greatly activated with increasing PASP dosage in this study (Supplementary Table S5). This result indicates that sufficient K was provided for the growth of *B. pilosa* under PASP addition, but the specific mechanism of K activation is unknown and needs further exploration. These results indicate that PASP

has various activation effects on different elements in the soils, which may be related to the fractional compositions of elements in the original soils.

Rhizospheric microbial communities strongly influence the physiology and development of plants (Kumawat et al., 2022). In this study, although PASP scarcely affected the overall microbial diversity and richness in the rhizospheric soils of *B. pilosa* (Supplementary Table S7), the abundance of some bacterial taxa markedly changed ($p < 0.05$) under PASP addition (Fig. 5). Similar phenomena have also been observed in several previous studies (Li et al., 2021b, 2022a), which can be attributed to the reduction of bacteria sensitive to the soil environment but the proliferation of tolerant bacteria. Changes in the abundance of these bacterial taxa were closely related to PASP in soils according to the RDA results (Fig. 4). The results corroborated several recent reports that the addition of soil chelators, such as EDTA, ethylenediamine disuccinic acid, citric acid (CA), and oxalic acid, could affect the soil bacterial community (Liang et al., 2019; Huang et al., 2021). Nevertheless, this study provides a deeper analysis of the driving factors of soil microbial community dynamics and their effects on plant response to Cd. The results showed that many rhizobacteria, such as *Sphingopyxis*, *Sphingomonas*, *Cupriavidus*, *Achromobacter*, *Nocardioides*, *Rhizobium*, *Variovorax*, *Burkholderia*, *Pseudomonas*, and *Pandoraea*, enriched in 3P and/or 6P soils (Fig. 6) were important PGPR (Aeron et al., 2020; Efe, 2020; Chen et al., 2021). These PGPR recruited by PASP, especially those with relatively high abundance (e.g., *Sphingopyxis, Sphingomonas, Cupriavidus, Achromobacter,* and *Nocardioides*) (Fig. 6), can improve plant growth of *B. pilosa* under Cd stress through various mechanisms, such as the production of phytohormones, siderophores, 1-aminocyclopropane-1-carboxylate deaminase, volatile organic compounds, biological N fixation, phosphate solubilization, and antifungal activity (Hakim et al., 2021). Moreover, the abundance of several potential K solubilizing rhizobacteria (KSR), including *Sphingomonas, Cupriavidus, Rhizobium*, *Burkholderia*, and *Pseudomonas* (Sattar et al., 2019; Han et al., 2021), was upregulated under PASP addition (Fig. 6), which can partially explain the increase in AK concentration in the soils (Supplementary Table S5). These results indicate that the remodelling of rhizobacteria by PASP may also play an important role in enhancing plant growth, in addition to the direct activation of nutrients by PASP (Hu et al., 2019). Based on this, combining PASP and the aforementioned PGPR may further improve the Cd phytoextraction efficiency by hyperaccumulators.

4.3. Mechanisms of enhanced Cd uptake by B. pilosa under PASP addition

In this study, PASP addition significantly promoted Cd uptake by *B. pilosa* (Fig. 1d−g), but the decrease ($p < 0.05$) in Cd TFs of *B. pilosa* after PASP addition (Supplementary Fig. S1c) suggests that PASP greatly improves Cd entry into plant roots but has a smaller contribution to Cd transport from roots to shoots. The results partially agreed with a similar study conducted in rapeseed, in which the authors considered that inhibiting Cd transportation from roots was a significant strategy for PASP alleviating Cd stress in rapeseed leaves (Wu et al., 2021b). The increased Cd accumulation should be attributed to the activated Cd bioavailability by PASP in soils (Wang et al., 2018), which can be achieved via acid dissolution, ion exchange, and surface complexation (Wang et al., 2020a).

However, in this study, the ACd concentrations in the 3P and 6P soils were not significantly higher than those in the 0P soil at the end of the experiment (Supplementary Table S5), although it showed a significantly positive correlation with PASP addition dosage (Supplementary Fig. S6). This can be interpreted as a result of trade-offs among soil Cd activation, Cd uptake by plants, and Cd immobilization through biological or physicochemical processes. The correlation analysis results (Supplementary Fig. S6) suggest that several soil indices (e.g., pH, EC, and AK concentration) have potential impacts on Cd availability, which may lead to changes in different Cd fractions, thereby determining Cd availability. This observation is consistent with the results of previous studies (Iranpour et al., 2014; de Anicésio and Monteiro, 2019; Yang et al., 2021). Among these soil indices, the high increase in AK concentration (Supplementary Table S5) after PASP addition has attracted substantial attention. Soil K concentration can affect Cd migration and transportation in soil–plant systems (de Anicésio and Monteiro, 2019; Shi et al., 2020a; He et al., 2021). Although Shi et al. (2020a) found that an increase in total K and AK concentrations in the soil was negatively correlated with bioavailable Cd concentrations in the soil and Cd concentrations in *Panax notoginseng*, de Anicésio and Monteiro (2019) reported that K fertilizers improve NH_4NO_3-extractable Cd concentrations in soils and Cd concentrations in plants. A recent study found that enhanced K^+ concentrations induce the upregulation of Cd^{2+} transporting proteins and downregulation of Cd^{2+} efflux proteins to increase Cd uptake by *Microcystis aeruginosa* (He et al., 2021). These studies suggest that the increase in AK likely played a role in improving Cd uptake by *B. pilosa*.

Soil microorganisms also play important roles in the regulation of Cd bioavailability. In this study, several PGPR (e.g., *Sphingomonas*, *Cupriavidus*, *Achromobacter*, *Rhizobium*, *Burkholderia*, and *Pseudomonas*) enriched in 3P and/or 6P soils (Fig. 6) are likely involved in immobilizing/mobilizing Cd in soils according to previous reports (Rajkumar et al., 2010; Wang et al., 2019; Zhang et al., 2019b; Shi et al., 2020b; Wu et al., 2020). Inoculation with *Sphingomonas* SaMR12 (Wang et al., 2019), *Cupriavidus* sp. WS2 (Shi et al., 2020b), *Achromobacter* sp. ZXH21 (Zhang et al., 2019b), and *Burkholdria* SaMR10 (Wang et al., 2019) have been found to modulate the uptake of various heavy metals by different plants. Many *Pseudomonas* species/stains have been shown to enhance heavy metal uptake by plants (Wu et al., 2020; Wang et al., 2021a), although several species and stains have been reported to immobilize heavy metals (Shahid et al., 2017). *Rhizobium* can improve the absorption of various heavy metals (e.g., Cd and Pb) by plants by releasing small organic molecules (e.g., phytosiderophores) to form complexes with them (Rajkumar et al., 2010). Interestingly, almost all of these PGPR involved in immobilizing/mobilizing Cd are potential KSR (Fig. 6). These results indicate multiple interactions between Cd and K in the soils.

4.4. Cd detoxification processes in B. pilosa under PASP addition

In this study, the plant growth of *B. pilosa* significantly increased under PASP addition despite the higher Cd concentrations in plants (Fig. 1), indicating that effective Cd detoxification processes were stimulated in *B. pilosa* plants. The potential mechanisms (e.g., chelation and antioxidant processes) of Cd detoxification in *B. pilosa* were analysed and discussed according to the physiological and metabolic results.

The change in antioxidant enzyme activity can be regarded as an indicator of plants fighting against heavy metal stresses (Li et al., 2021c; Wu et al., 2021b). Several antioxidant enzymes can effectively scavenge reactive oxygen species (ROS) accumulation under Cd stress (Li et al., 2018). In this study, the activities of SOD and CAT significantly increased ($p < 0.05$) in the 6P group compared to those in the 0P group (Supplementary Figs. S2a and b), suggesting that these enzymes are involved in the scavenging of ROS (e.g., H_2O_2 and O_2^-) on the basis of their catalytic functions (Li et al., 2021c). Similar concentrations of the lipid peroxide MDA, an indicator of oxidative stress in cells (Hnilickova et al., 2021), in the three groups (Supplementary Fig. S2c) directly indicated the effective antioxidant process in the leaves of *B. pilosa*. The results were consistent with a previous study (Wu et al., 2021b), in which the authors found that PASP can alleviate Cd toxicity in rapeseed leaves by activating the antioxidant system.

Amino acids in plants can contribute to Cd detoxification by regulating ion transport, ion chelation, and N metabolism under heavy metal stress (Wang et al., 2020c). In this study, most (> 80%) of the differential amino acids were upregulated under PASP addition (Fig. 2d and

e). The increase in these amino acids under PASP addition may be closely related to the increase in N intake and likely participate in various metabolic processes. Moreover, some of them (e.g., proline, histidine, and methionine) should play important roles in Cd detoxification (Wang et al., 2020b). Proline is involved in Cd detoxification by directly adjusting osmotic potential and serving as an antioxidant or through the biosynthesis of chelating peptides (Borgo et al., 2021; de la Torre et al., 2022). Histidine is involved in the chelation and transport of metal ions (Xu et al., 2012; Kato et al., 2020). For example, Xu et al. (2012) found that a high accumulation of histidine promoted Cd uptake and root-to-shoot transport in *Solanum* species. Methionine, as the precursor of compounds associated with antioxidant defense (e.g., polyamines) and metal homeostasis (e.g., nicotinamide), is also likely to be involved in protecting plants against Cd toxicity (Kato et al., 2020). In this study, the relative abundance of these three amino acids increased several times under PASP addition (Supplementary Tables S3 and S4), indicating their important roles in Cd detoxification in *B. pilosa*. Additionally, the increase in some other amino acids (e.g., aspartic acid, lysine, glutamine, tryptophan, and arginine) (Supplementary Tables S3 and S4) may also have multiple effects on Cd tolerance in *B. pilosa*, which were also induced by Cd in other plants (Li et al., 2018; Mengdi et al., 2020).

Organic acids, which are mainly produced in the mitochondria through the tricarboxylic acid cycle, are an important class of metal ligands in plants and participate in the absorption, transportation, storage, and detoxification of heavy metals (Yang et al., 2020). In this study, the increase in malic acid (MA) abundance after the addition of 3 g kg^{-1} PASP (Supplementary Table S3 and Table S4) likely plays an important role in Cd detoxification in *B. pilosa* because MA and CA have been considered to be the main organic acids that chelate heavy metals in plants (Yang et al., 2020). Additionally, the induction of some other organic acids in *B. pilosa* (Fig. 2d and e) may also contribute to Cd tolerance in this study, although their specific functions are not clearly understood.

In addition to amino acids and organic acids, most (> 80%) of the differential lipids were also upregulated under PASP addition (Fig. 2d and e). A recent review indicates the possibility of membrane protein-lipid-metal ion interactions in regulating metal homeostasis in plant cells (Wu et al., 2021a). Lipids can act as metal ion recognizers to first sense metal ion stimulation, and then ion channels and transporters specifically bind to the metal ions to control their movements and activities (Wu et al., 2021a). These previous findings suggest that the upregulated lipids in this study are also likely involved in plant responses to Cd, but the specific functions of different lipids need to be further explored.

5. Conclusions

This study found that the Cd phytoextraction efficiency of *B. pilosa* was promoted by 46.4% and 76.4% upon the addition of 3 and 6 mg kg^{-1} PASP in soils, respectively, owing to its Cd activation and plant growth-promoting effect. PASP recruited many PGPR to promote plant growth under Cd stress, and some of these PGPR were involved in Cd mobility and likely contributed to Cd uptake by *B. pilosa*. Notably, the increased AK concentrations in the rhizosphere, which were activated by PASP and/or KSR, might also assist in plant growth and Cd uptake in *B. pilosa*. Moreover, PASP induced plants to initiate complex Cd detoxification processes involving antioxidant enzymes, amino acids, organic acids, and lipids to improve Cd-bearing capacity. This study provides comprehensive insight into understanding the mechanisms of PASP for enhancing Cd phytoextraction efficiency. The results suggest that the combination of PASP-PGPR and/or PASP-K fertilizer can be employed to further enhance the Cd phytoextraction efficiency. However, further research is warranted on this topic. For example, the effect of PASP on plant root exudates and its relationship with Cd availability and microbial community composition in the soil have not yet been revealed. In addition, whether the mechanisms uncovered in this study have similarities in different soil–heavy metal–plant systems needs to be determined in future studies.

Credit author statement

Xiong Li: Conceptualization, Methodology, Validation, Formal analysis, Investigation, Writing – original draft, Writing – review & editing, Visualization, Supervision, Funding acquisition. **Liyan Tian**: Methodology, Formal analysis, Investigation, Writing – review & editing, Visualization. **Boqun Li**: Formal analysis, Investigation, Writing – review & editing. **Huafang Chen**: Methodology, Formal analysis, Investigation, Writing – review & editing. **Gaojuan Zhao**: Validation, Investigation, Writing – review & editing. **Xiangshi Qin**: Investigation. **Yuanyuan Liu**: Investigation, Writing – review & editing. **Yongping Yang**: Conceptualization, Writing – review & editing, Supervision. **Jianchu Xu**: Conceptualization, Writing – review & editing, Supervision.

Declaration of competing interest

The authors declare that they have no known competing financial interests or personal relationships that could have appeared to influence the work reported in this paper.

Data availability

I have shared the link to my data at the Attach Files step.

Acknowledgments

This work was funded by the Youth Innovation Promotion Association CAS (2020387), the Key Project of Yunnan Provincial Science and Technology Department (202101AS070045), and the Strategic Priority Research Program of Chinese Academy of Sciences (XDA2602020).

Appendix A. Supplementary data

Supplementary data to this article can be found online at https://doi.org/10.1016/j.chemosphere.2022.136068.

References

Aeron, A., Khare, E., Jha, C.K., Meena, V.S., Aziz, S.M.A., Islam, M.T., Kim, K., Meena, S. K., Pattanayak, A., Rajashekara, H., Dubey, R.C., Maurya, B.R., Maheshwari, D.K., Saraf, M., Choudhary, M., Verma, R., Meena, H.N., Subbanna, A., Parihar, M., Shukla, S., Muthusamy, G., Bana, R.S., Bajpai, V.K., Han, Y.K., Rahman, M., Kumar, D., Singh, N.P., Meena, R.K., 2020. Revisiting the plant growth-promoting rhizobacteria: lessons from the past and objectives for the future. Arch. Microbiol. 202, 665–676.

Arshad, M., Naqvi, N., Gul, I., Yaqoob, K., Bilal, M., Kallerhoff, J., 2020. Lead phytoextraction by *Pelargonium hortorum*: comparative assessment of EDTA and DIPA for Pb mobility and toxicity. Sci. Total Environ. 748, 141496.

Borgo, L., Rabêlo, F.H.S., Budzinski, I.G.F., Cataldi, T.R., Ramires, T.G., Schaker, P.D.C., Ribas, A.F., Labate, C.A., Lavres, J., Cuypers, A., Azevedo, R.A., 2021. Proline exogenously supplied or endogenously overproduced induces different nutritional, metabolic, and antioxidative responses in transgenic tobacco exposed to cadmium. J. Plant Growth Regul. https://doi.org/10.1007/s00344-021-10480-6.

Cao, D., Wang, S.Z., Han, M., 2021. Effect of the environment-friendly nutrient synergist polyaspartic acid on the growth of poplar seedlings. Bull. Bot. Res. 41, 712–720.

Cha, L.J., Zhao, S.Y., Feng, H.J., Zhou, D.D., 2020. Study on influencing factors of heavy metal forms in wild fungi growth soil. Ecol. Environ. Sci. 29, 2457–2464.

Chen, W., Gong, L., Guo, Z., Wang, W., Zhang, H., Liu, X., Yu, S., Xiong, L., Luo, J., 2013. A novel integrated method for large-scale detection, identification, and quantification of widely targeted metabolites: application in the study of rice metabolomics. Mol. Plant 6, 1769–1780.

Chen, Z.J., Tian, W., Li, Y.J., Sun, L.N., Chen, Y., Zhang, H., Li, Y.Y., Han, H., 2021. Responses of rhizosphere bacterial communities, their functions and their network interactions to Cd stress under phytostabilization by *Miscanthus* spp. Environ. Pollut. 287, 117663.

de Anicésio, É.C.A., Monteiro, F.A., 2019. Potassium affects the phytoextraction potential of *Tanzania guinea* grass under cadmium stress. Environ. Sci. Pollut. Res. 26, 30472–30484.

de la Torre, V.G.S., de la Peña, T.C., Lucas, M.M., Pueyo, J.J., 2022. Transgenic *Medicago truncatula* plants that accumulate proline display enhanced tolerance to cadmium stress. Front. Plant Sci. 13, 829069.
Deng, F., Wang, L., Mei, X.F., Li, S.X., Pu, S.L., Li, Q.P., Ren, W.J., 2019. Polyaspartic acid (PASP)-urea and optimised nitrogen management increase the grain nitrogen concentration of rice. Sci. Rep. 9, 313.
Dolev, N., Katz, Z., Ludmer, Z., Ullmann, A., Brauner, N., Goikhman, R., 2020. Natural amino acids as potential chelators for soil remediation. Environ. Res. 183, 109140.
Efe, D., 2020. Potential plant growth-promoting bacteria with heavy metal resistance. Curr. Microbiol. 77, 3861–3868.
Guan, X.F., Xu, Q.X., Lin, B.F., Qian, L., Lin, B., 2017. Correlation analysis of fruit quality, soil elements and microorganisms in navel orange orchard. Chinese Agric. Sci. Bull. 33, 69–76.
Hakim, S., Naqqash, T., Nawaz, M.S., Laraib, I., Siddique, M.J., Zia, R., Mirza, M.S., Imran, A., 2021. Rhizosphere engineering with plant growth-promoting microorganisms for agriculture and ecological sustainability. Front. Sustain. Food Syst. 5, 617157.
Han, M., Zhu, X.Y., Chen, G.W., Wan, X.M., Wang, G., 2021. Advances on potassium-solubilizing bacteria and their microscopic potassium solubilizing mechanisms. Acta Pedol. Sin. 1–15.
He, X., Zhang, J., Ren, Y., Sun, C., Deng, X., Qian, M., Hu, Z., Li, R., Chen, Y., Shen, Z., Xia, Y., 2019. Polyaspartate and liquid amino acid fertilizer are appropriate alternatives for promoting the phytoextraction of cadmium and lead in *Solanum nigrum* L. Chemosphere 237, 124483.
He, Y.X., Liu, M.Z., Wang, R.L., Salam, M., Yang, Y.C.A., Zhang, Z.X., He, Q., Hu, X.B., Li, H., 2021. Potassium regulates cadmium toxicity in *Microcystis aeruginosa*. J. Hazard Mater. 413, 125374.
Hnilickova, H., Kraus, K., Vachova, P., Hnilicka, F., 2021. Salinity stress affects photosynthesis, malondialdehyde formation, and proline content in *Portulaca oleracea* L. Plants (Basel) 10, 845.
Hou, T., Yu, S.S., Zhou, M.F., Wu, M., Liu, J., Zheng, X.L., Li, J.X., Wang, J., Wang, X.L., 2020. Effective removal of inorganic and organic heavy metal pollutants with poly (amino acid)-based micromotors. Nanoscale 12, 5227–5232.
Hu, M.M., Dou, Q.H., Cui, X.M., Lou, Y.H., Zhuge, Y.P., 2019. Polyaspartic acid mediates the absorption and translocation of mineral elements in tomato seedlings under combined copper and cadmium stress. J. Integr. Agric. 18, 1130–1137.
Huang, R., Cui, X., Luo, X., Mao, P., Zhuang, P., Li, Y., Li, Y., Li, Z., 2021. Effects of plant growth regulator and chelating agent on the phytoextraction of heavy metals by *Pfaffia glomerata* and on the soil microbial community. Environ. Pollut. 283, 117159.
Iranpour, M., lakzian, A., Khorasani, R., 2014. Effects of cadmium and organic matter on soil pH, electrical conductivity and their roles in cadmium availability in soil. J. Middle East Appl. Sci. Technol 643–646.
Ji, P.T., Li, X.L., Peng, Y.J., Zhang, Y.C., Tao, P.J., 2021. Effect of polyaspartic acid and different dosages of controlled-release fertilizers on nitrogen uptake, utilization, and yield of maize cultivars. Bioengineered 12, 527–539.
Kato, F.H., Carvalho, M.E.A., Gaziola, S.A., Azevedo, R.A., 2020. Maize plants have different strategies to protect their developing seeds against cadmium toxicity. Theor. Exp. Plant Phys. 32, 203–211.
Khanna, K., Jamwal, V.L., Kohli, S.K., Gandhi, S.G., Ohri, P., Bhardwaj, R., Abdjtllah, E. F., Hashem, A., Ahmad, P., 2019. Plant growth promoting rhizobacteria induced Cd tolerance in *Lycopersicon esculentum* through altered antioxidative defense expression. Chemosphere 217, 463–474.
Kumawat, K.C., Razdan, N., Saharan, K., 2022. Rhizospheric microbiome: bio-based emerging strategies for sustainable agriculture development and future perspectives. Microbiol. Res. 254, 126901.
Li, F.Z., Zhang, Y.P., Hao, S.F., Xu, W.W., Shen, K., Long, Z., 2020a. Leaching behaviour and enhanced phytoextraction of additives for cadmium-contaminated soil by *Pennisetum* sp. Bull. Environ. Contam. Toxicol. 104, 658–667.
Li, Q., Song, J., 2019. Analysis of widely targeted metabolites of the euhalophyte *Suaeda salsa* under saline conditions provides new insights into salt tolerance and nutritional value in halophytic species. BMC Plant Biol. 19, 388.
Li, X., Chen, D., Li, B.Q., Yang, Y., Yang, Y.P., 2021a. Combined transcriptomic, proteomic and biochemical approaches to identify the cadmium hyper-tolerance mechanism of turnip seedling leaves. Environ. Sci. Pollut. Res. 28, 22458–22473.
Li, X., Chen, D., Li, B.Q., Yang, Y.P., 2021b. Cd accumulation characteristics of *Salvia tiliifolia* and changes of rhizospheric soil enzyme activities and bacterial communities under a Cd concentration gradient. Plant Soil 463, 225–247.
Li, X., Chen, D., Yang, Y., Liu, Y., Luo, L., Chen, Q., Yang, Y., 2021c. Comparative transcriptomics analysis reveals differential Cd response processes in roots of two turnip landraces with different Cd accumulation capacities. Ecotoxicol. Environ. Saf. 220, 112392.
Li, X., Li, B.Q., Zheng, Y., Luo, L.D., Qin, X.S., Yang, Y.P., Xu, J.C., 2022a. Physiological and rhizospheric response characteristics to cadmium of a newly identified cadmium accumulator *Coreopsis grandiflora* Hogg. (Asteraceae). Ecotoxicol. Environ. Saf. 241, 113739.
Li, X., Yang, Y.P., 2020. Preliminary study on Cd accumulation characteristics in *Sansevieria trifasciata* Prain. Plant Divers. 42, 351–355.
Li, X., Zhang, X.M., Li, B.Q., Wu, Y.S., Sun, H., Yang, Y.P., 2017. Cadmium phytoremediation potential of turnip compared with three common high Cd-accumulating plants. Environ. Sci. Pollut. Res. 24, 21660–21670.
Li, X., Zhang, X.M., Wu, Y.S., Li, B.Q., Yang, Y.P., 2018. Physiological and biochemical analysis of mechanisms underlying cadmium tolerance and accumulation in turnip. Plant Divers. 40, 19–27.
Li, Y.J., Ma, J.W., Li, Y.Q., Xiao, C., Shen, X.Y., Chen, J.J., Xia, X.H., 2022b. Nitrogen addition facilitates phytoremediation of PAH-Cd cocontaminated dumpsite soil by altering alfalfa growth and rhizosphere communities. Sci. Total Environ. 806, 150610.
Li, Z.J., Shen, Y.X., Zhao, G.J., Yu, Z.F., Chen, F.J., Xiao, G.Y., 2020b. Changes of soil fungi and bacteria after forest mother soil transplantation. Microbiol. China 47, 3196–3205.
Liang, Y., Wang, X., Guo, Z., Xiao, X., Peng, C., Yang, J., Zhou, C., Zeng, P., 2019. Chelator-assisted phytoextraction of arsenic, cadmium and lead by *Pteris vittata* L. and soil microbial community structure response. Int. J. Phytoremediation 21, 1032–1040.
Liu, X.Y., Mao, Y., Zhang, X.Y., Gu, P.X., Niu, Y.H., Chen, X.L., 2019. Effects of PASP/NTA and TS on the phytoremediation of pyrene-nickel contaminated soil by *Bidens pilosa* L. Chemosphere 237, 124502.
Manoj, S.R., Karthik, C., Kadirvelu, K., Arulselvi, P.I., Shanmugasundaram, T., Bruno, B., Rajkumar, M., 2020. Understanding the molecular mechanisms for the enhanced phytoremediation of heavy metals through plant growth promoting rhizobacteria: a review. J. Environ. Manag. 254, 109779.
Mengdi, X., Haibo, D., Jiaxin, L., Zhe, X., Yi, C., Xuan, L., Haiyan, M., Hui, S., Tianqi, A., Yunzhen, L., Wenqing, C., 2020. Metabolomics reveals the "Invisible" detoxification mechanisms of *Amaranthus hypochondriacus* at three ages upon exposure to different levels of cadmium. Ecotoxicol. Environ. Saf. 195, 110520.
Mu'azu, N.D., Haladu, S.A., Jarrah, N., Zubair, M., Essa, M.H., Ali, S.A., 2018. Polyaspartate extraction of cadmium ions from contaminated soil: evaluation and optimization using central composite design. J. Hazard Mater. 342, 58–68.
Rajkumar, M., Ae, N., Prasad, M.N., Freitas, H., 2010. Potential of siderophore-producing bacteria for improving heavy metal phytoextraction. Trends Biotechnol. 28, 142–149.
Reeves, R.D., Baker, A.J.M., Jaffre, T., Erskine, P.D., Echevarria, G., van der Ent, A., 2018. A global database for plants that hyperaccumulate metal and metalloid trace elements. New Phytol. 218, 407–411.
Sattar, A., Naveed, M., Ali, M., Zahir, Z.A., Nadeem, S.M., Yaseen, M., Meena, V.S., Farooq, M., Singh, R., Rahman, M., Meena, H.N., 2019. Perspectives of potassium solubilizing microbes in sustainable food production system: a review. Appl. Soil Ecol. 133, 146–159.
Shahid, M., Dumat, C., Khalid, S., Niazi, N.K., Antunes, P.M.C., 2017. Cadmium bioavailability, uptake, toxicity and detoxification in soil-plant system. In: Reviews of Environmental Contamination and Toxicology. Springer, New York, pp. 73–137.
Shi, Y., Pu, R.F., Guo, L.P., Man, J.H., Shang, B.P., Ou, X.H., Dai, C.Y., Liu, P.F., Cui, X. M., Ye, Y., 2020a. Formula fertilization of nitrogen and potassium fertilizers reduces cadmium accumulation in *Panax notoginseng*. Arch. Agron Soil Sci. 66, 343–357.
Shi, Z., Zhang, Z., Yuan, M., Wang, S., Yang, M., Yao, Q., Ba, W., Zhao, J., Xie, B., 2020b. Characterization of a high cadmium accumulating soil bacterium. *Cupriavidus* sp. WS2. Chemosphere 247, 125834.
Thinh, N.V., Osanai, Y., Adachi, T., Vuong, B.T.S., Kitano, I., Chung, N.T., Thai, P.K., 2021. Removal of lead and other toxic metals in heavily contaminated soil using biodegradable chelators: GLDA, citric acid and ascorbic acid. Chemosphere 263, 127912.
Wang, G., Zhang, S., Zhong, Q., Xu, X., Li, T., Jia, Y., Zhang, Y., Peijnenburg, W., Vijver, M.G., 2018. Effect of soil washing with biodegradable chelators on the toxicity of residual metals and soil biological properties. Sci. Total Environ. 625, 1021–1029.
Wang, G.Y., Pan, X.M., Zhang, S.R., Zhong, Q.M., Zhou, W., Zhang, X.H., Wu, J., Vijver, M.G., Peijnenburg, W.J.G.M., 2020a. Remediation of heavy metal contaminated soil by biodegradable chelator-induced washing: efficiencies and mechanisms. Environ. Res. 186, 109554.
Wang, J.Y., Li, M., Song, X.H., Li, Q., qi, X.F., Wang, L.L., 2020b. The application of metabonomics in study of plant under heavy metal stress. Biol. Chem. Eng. 6, 128–132.
Wang, Q., Ma, L., Zhou, Q., Chen, B., Zhang, X., Wu, Y., Pan, F., Huang, L., Yang, X., Feng, Y., 2019. Inoculation of plant growth promoting bacteria from hyperaccumulator facilitated non-host root development and provided promising agents for elevated phytoremediation efficiency. Chemosphere 234, 769–776.
Wang, R.Z., Hou, D.D., Chen, J.Z., Li, J.H., Fu, Y.Y., Wang, S., Zheng, W., Lu, L.L., Tian, S. K., 2020c. Distinct rhizobacterial functional assemblies assist two *Sedum alfredii* ecotypes to adopt different survival strategies under lead stress. Environ. Int. 143, 105912.
Wang, X.L., de Souza, M.F., Li, H.C., Qiu, J., Ok, Y.S., Meers, E., 2022. Biodegradation and effects of EDDS and NTA on Zn in soil solutions during phytoextraction by alfalfa in soils with three Zn levels. Chemosphere 292, 133519.
Wang, Y., Yang, R., Hao, J.J., Sun, M.Q., Wang, H.Y., Ren, H.J., 2021a. The impact of *Pseudomonas monteilii* PN1 on enhancing the alfalfa phytoextraction and responses of rhizosphere soil bacterial communities in cadmium-contaminated soil. J. Environ. Chem. Eng. 9, 106533.
Wang, Y.Y., Li, S.F., Wang, X.S., Xu, J.F., Li, T.T., Zhu, J., Yang, R.Y., Wang, J.S., Chang, M., Wang, L., 2021b. Biochelator assisted phytoremediation for cadmium (Cd) pollution in paddy field. Sustainability (Basel) 13, 12170.
Wu, D., Saleem, M., He, T., He, G., 2021a. The mechanism of metal homeostasis in plants: a new view on the synergistic regulation pathway of membrane proteins, lipids and metal ions. Membranes (Basel) 11, 984.
Wu, M.X., Luo, Q., Liu, S.L., Zhao, Y., Long, Y., Pan, Y.Z., 2018. Screening ornamental plants to identify potential Cd hyperaccumulators for bioremediation. Ecotoxicol. Environ. Saf. 162, 35–41.
Wu, X., Tian, H., Li, L., Wang, X., 2021b. Polyaspartic acid alleviates cadmium toxicity in rapeseed leaves by affecting cadmium translocation and cell wall fixation of cadmium. Ecotoxicol. Environ. Saf. 224, 112685.
Wu, Y.J., Ma, L.Y., Liu, Q.Z., Sikder, M.M., Vestergard, M., Zhou, K.Y., Wang, Q., Yang, X., Feng, Y., 2020. *Pseudomonas fluorescens* promote photosynthesis, carbon

fixation and cadmium phytoremediation of hyperaccumulator *Sedum alfredii*. Sci. Total Environ. 726, 138554.
Xie, S.Y., Ling, D.X., Wang, P., Cao, J.J., Luo, S.Y., Wu, H.P., 2021. Effect of PASP and NAA coupling on extraction of cadmium from *Sorghum dochna* (Forssk.) Snowden. J. Central South Univ. For. Technol. 42, 1–8.
Xu, J., Zhu, Y.Y., Ge, Q., Li, Y.L., Sun, J.H., Zhang, Y., Liu, X.J., 2012. Comparative physiological responses of *Solanum nigrum* and *Solanum torvum* to cadmium stress. New Phytol. 196, 125–138.
Yang, J.H., Liu, T., Chen, Y.X., Wang, M., Wang, H.Y., Liu, H.B., 2018. Synthesis, modification and application of polyaspartic acid/salt: the state-of-art technological advances. Mater. Rep. 32, 1852–1862.
Yang, X.Y., Wang, H.J., Wang, H.B., 2020. Advances in physiological and molecular mechanisms of cadmium hyperaccumulation by *Solanum nigrum* L. Asian J. Ecotoxicol. 15, 72–81.
Yang, Y., Li, Y., Wang, M., Chen, W., Dai, Y., 2021. Limestone dosage response of cadmium phytoavailability minimization in rice: a trade-off relationship between soil pH and amorphous manganese content. J. Hazard Mater. 403, 123664.
Yu, G., Liu, J., Long, Y., Chen, Z., Sunahara, G.I., Jiang, P., You, S., Lin, H., Xiao, H., 2020. Phytoextraction of cadmium-contaminated soils: comparison of plant species and low molecular weight organic acids. Int. J. Phytoremediat. 22, 383–391.
Yuan, C.P., Gao, B.L., Peng, Y.T., Gao, X., Fan, B.B., Chen, Q., 2021. A meta-analysis of heavy metal bioavailability response to biochar aging: importance of soil and biochar properties. Sci. Total Environ. 756, 144058.
Zhang, H.X., Liang, P.X., Li, Y.L., Shan, J.L., Tan, L.T., 2019a. Single and complex green chelates: effect on the enrichment of cadmium and arsenic in *Amaranthus mangostanus* L. Chinese Agric. Sci. Bull. 35, 112–118.
Zhang, X., Shi, L.J., Liu, X.Y., Zhang, H., Li, L.H., Tan, T.W., Cao, H., 2013. The research of enhancing phytoremediation of heavy metals contaminated soil with PASP. Chinese Agric. Sci. Bull. 29, 151–156.
Zhang, X.H., Sun, B., Wei, Z.M., Zhao, C.Y., Xu, Y.Z., Zhang, L.H., Xu, L., 2019b. Screening of two cadmium tolerant microorganisms and their differences in adsorption and immobilization of cadmium. J. Nanjing Agric. Univ. 42, 869–876.
Zhang, X.Y., Gu, P.X., Liu, X.Y., Huang, X., Wang, J.Y., Zhang, S.Y., Ji, J.H., 2021. Effect of crop straw biochars on the remediation of Cd-contaminated farmland soil by hyperaccumulator *Bidens pilosa* L. Ecotoxicol. Environ. Saf. 219, 112332.
Zhang, Y.P., Li, F.Z., Xu, W.W., Ren, J.H., Chen, S.H., Shen, K., Long, Z., 2019c. Enhanced phytoextraction for co-contaminated soil with Cd and Pb by ryegrass (*Lolium perenne* L.). Bull. Environ. Contam. Toxicol. 103, 147–154.
Zhao, M., Ren, Y., Wei, W., Yang, J., Zhong, Q., Li, Z., 2021. Metabolite analysis of jerusalem artichoke (*Helianthus tuberosus* L.) seedlings in response to polyethylene glycol-simulated drought stress. Int. J. Mol. Sci. 22, 3294.